Research Article

Journal of Environmental Nanotechnology

Developing Dynamic System Responses Model Based on Nanotechnology by Incorporating the Finite Element Analysis

M. Dawood* and S. P. Kumar

Department of Mechanical Engineering, Sam Higginbottom University of Agriculture, Technology and Sciences, Prayagraj, UP, India

Received: 20.02.2024 Accepted: 20.03.2024 Published: 30.03.2024

*mohddowood@gmail.com

ABSTRACT

The dynamic model of complex structure has set incredible progression with the use of finite element analysis (FEA), especially in the field of vibration control and nanotechnology. Main focus of this research is to conduct a frequency analysis in ANSYS and a state space model of the beam under the platform of MATLAB. This allowed a system to develop an active dynamic model for vibration control. To enhance test and analysis of the cantilever beam of Aluminium 6061T6, a new method has been proposed to predict the dynamic response of a cantilever beam under sinusoidal base excitation. This was achieved by creating an analytical model for the cantilever beam using moment and force equilibrium equations. The authenticity of the proposed method was made by comparing the results with experimental data. Additionally, to control vibration, a Proportional-Integral-Derivative (PID) controller was developed using the system model. The FEA in the ANSYS platform provided a cantilever beam model. Also, its mathematical modelling has been done. The proposed method utilizes a novel disturbance rejection control scheme that eliminates an unknown disturbance. Experimental results indicate that the control system results in gradually decreased beam vibration amplitude. The state space approach discussed in the work could be a valuable tool for studying the behaviours of nanomaterials.

Keywords: Aluminium 6061T6 beam; Active dynamic vibration control; PID controller; State space model.

1. INTRODUCTION

Vibrations are a common occurrence in mechanical and structural systems. However, if left unchecked, they could lead to disastrous results. Vibration control of the smart structure is realized through four piezo ceramic PZT actuators and one PZT sensor bonded to the plate (Kozupa and Wiciak, 2010). Piezoelectric materials are commonly used as sensors and actuators in smart structures due to simple desirable properties (Rahman and Alam, 2015). Hybrid composite and sandwich plates with some distributed, surface-bonded and/or embedded piezoelectric sensors and actuators are now widely used in active vibration, acoustic, shape and position control applications (Kapuria and Kulkarni, 2008). Structures are subjected to varying temperature conditions that often induce thermal distortions. Thermal stresses may sometimes induce buckling and dynamic instability in thin-walled composite structures (Rahman and Alam, 2015). Flexible-joint manipulators (FJM) offer several advantages with respect to their rigid counterpart, such as light weight, lower cost, smaller actuators, work volume, better manoeuvrability and transportability, higher operational speed, power efficiency, and larger number applications (Khalil and Abdel, 2018). The term of flexible structure is customarily used within the control engineering community to refer to a system with oscillatory properties that is characterized by a strong amplification of a harmonic signal for resonant frequencies (Rahman and Darus, 2011). A smart structure is a system which has built in or intrinsic sensors, actuators and control mechanism whereby it is capable of sensing a stimulus, responding to it in a predetermined manner in a short/appropriate time so as to revert to its original state as soon as the stimulus is removed (Heganna and Joglekar, 2016). Active vibration control is the process of using smart materials for controlling vibrations in real time (Khot *et al.* 2012). A smart structure typically consists of a host structure incorporated with sensors and actuators coordinated by a controller (Rahman and Alam, 2012). Light structures are generally less rigid, so they are more susceptible to excessive vibration problems (Qiu *et al.* 2009). Advanced lightweight structural systems have been achieved in various research fields with the aid of high technologies in computer and material sciences. Especially, the emergence of so-called smart materials has accelerated successful development of the advanced structural systems (Choi and Sohn, 2006). The theory of active control of flexible structures is a well-established technique. This may be achieved either by feedforward or feedback control strategies (Gatti *et al.* 2007). A beam is a slender horizontal structural member that resists

lateral loads by bending, and this important element of engineering structures appears in various forms (Avcar, 2014). Base excitation is an important way to test vibration parameters of a structure (Wei, 2010). Smart materials are new generation materials surpassing the conventional structural and functional materials. These materials possess adaptive capabilities to external stimuli, such as loads or environment, with inherent intelligence (Kamile, 2013). At the nanoscale, material scientists have demonstrated the ability to design entirely new materials molecule by molecule (Flatau and Chong, 2002). The critical deterioration of transportation infrastructure across the continent, including highways and bridges, has driven the search for new methods of concrete rehabilitation and repair (Krishna and Thirumal, 2015). Smart structure integrates the properties of embedded sensors, actuators and control mechanism in order to respond to a given stimulus in a functionally useful manner (Sukesha *et al.* 2014). Electrospun nanofibrous mats have a special fiber structure composed of continuous layers of numerous and long micro/nanofibers. The fibers constituting the nanofibrous mats are produced by high-voltage electrospinning, which uses high-voltage static electricity to produce a charged-polymer jet to stretch and thin the fibers in the electrostatic field (Yin and Xiong, 2018). Studies of nanoscale structures offer great promise but require new theoretical approaches and computationally intensive studies (Sarhan, 2013). Two primary methods of vibration control have emerged: active control systems and passive control systems. While passive control systems could mitigate vibrations to some extent, active control methods are more effective in eliminating undesired vibrations in engineering structures. Finite Element Analysis in Nanotechnology plays a crucial role in various fields such as electronics, micro computing, material science, quantum science, engineering, and biotechnology, and medicine, aerospace, and environmental and computational nanotechnology. The widely utilized finite element method (FEM) is essential for addressing challenges in both conventional engineering fields and Nano research, especially when experimental analysis is not feasible.

Applications of FEM in nanotechnology research includes i) study of electrospun nanofibrous mats under biaxial tension, ii) analysis of stress transfer in carbon nanotube reinforced composites and iii) development of 3D FEM for adhesive contact at nanoscale.

The primary objective of active vibration control is to reduce vibration levels in mechanical systems by modifying the structural response of the system directly and automatically. Active structures consist of a set of sensors to detect and measure responses, a set of actuators to influence structural responses, and controllers to process signals from the sensors to modify the system responses as required. Structures that have unique features such as distributed and high-level integration capability of actuators and sensors are often referred to as smart structures. The critical component of an active system is the actuator, which functions as an external excitation to affect the control system. Commonly used actuators in active control systems include hydraulic, pneumatic, electrodynamic or smart material actuators such as piezoelectric materials. Piezoelectric smart structures have enormous potential in engineering applications for active vibration control. To better understand the behaviour of dynamic systems, ANSYS and MATLAB software are used for modelling and response analysis. In a variety of fields namely, space and aircraft structures, satellites, cars, and bridges, unwanted vibrations could create major issues. The impact of these vibrations could range from minor annoyances like noise in machines or automobiles to create significant problems in the environment as well as in areas like space structures, where precise behaviour is essential and any deviation could lead to significant costs. As a result, vibration control is a vital area that requires attention. This paper presents a comprehensive analysis of the vibration response of a cantilever beam (Fig. 1) under base excitation. Experimental studies were conducted using an electrodynamic shaker as the controller actuator. Meshed uniform beam is shown in Fig. 2.

2. DESIGN CONSIDERATION AND THEORETICAL MODEL

2.1 Modal Analysis

The partial differential equation of motion for free vibration of an Euler-Bernoulli beam were given by

$$EI\frac{\partial^4 v(x,t)}{\partial x^4} + \rho A\frac{\partial^2 v(x,t)}{\partial t^2} = 0 \quad (1)$$

where A is the cross-sectional area, I is the moment of inertia of the cross-sectional area, E is the modulus of elasticity, ρ is the mass per unit of volume and $v(x,t)$ is the transverse deflection at the axial location x and at the time t. For a unique solution for $v(x,t)$, two initial equations and four boundary conditions are required because the equation of motion comprises of a second order derivative with respect to time and a fourth order derivative with respect to position. Equation of motion could be solved by using the methods of separation of variables and Eigen functions expansion. The transverse deflection $v(x,t)$ is separated into two functions as follows:

$$v(x,t) = V(x)T(t) \quad (2)$$

where $V(x)$ is known as the normal mode or characteristic function of the beam. Therefore, the Eq. (1) is rewritten as:

$$c^2 \frac{1}{V(x)} \frac{\partial^4 V(x)}{\partial x^4} = -\frac{1}{T(t)} \frac{\partial^2 T(t)}{\partial t^2} = \omega^2 \quad (3)$$

where $c = \sqrt{EI/\rho A}$ and ω is the natural frequency. Note that the left side of the Eq. (3) is in relation to position and the right side to time and both could be split into two equations

$$\frac{d^4 W(x)}{dx^4} - \beta^4 W(x) = 0 \quad (4)$$

$$\frac{d^2 T(t)}{dt^2} + \omega^2 T(t) = 0 \quad (5)$$

where β is the eigenvalue of the normal mode $V(x)$ and

$$\beta = \sqrt{\frac{\omega}{c}} \quad (6)$$

Solutions of $T(t)$ and $V(x)$ in Eq. (4) and Eq. (5), respectively, are given by:

$$T(t) = Dcos(\omega t - \varphi)$$

$$V(x) = C_1 \sin(\beta x) + C_2 \cos(\beta x) + C_3 \sin(\beta x) + C_4 \cosh(\beta x) \quad (7)$$

C_1, C_2, C_3 and C_4 are constants which could be found by using the appropriate boundary conditions, D is a constant which could be obtained by using initial conditions and ϕ was the phase angle. Modal analysis is the theme of solving any vibration problem. In this particular case, the validation of natural frequencies was the first step. The ANSYS software solves for Eigen values (i.e., natural frequencies) in the modal part of the system. We consider a uniform aluminium beam with dimensions of length, breadth, and height as 200 mm, 20 mm, and 4 mm, respectively. Table 1 shows the properties of the aluminium used in the simulation.

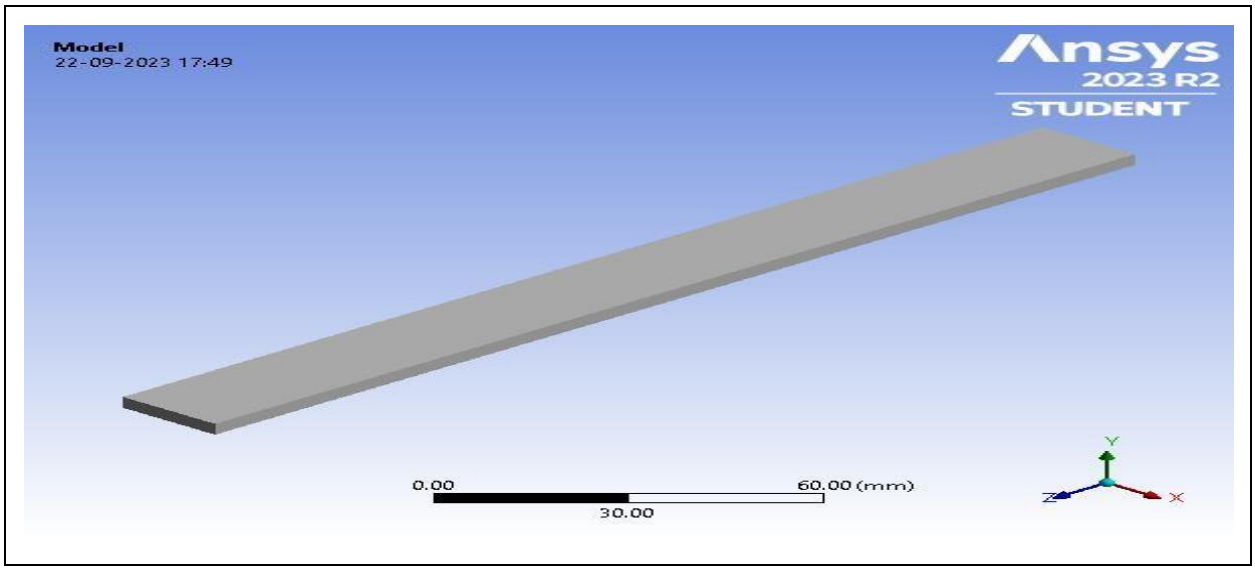

Fig. 1: Model of the beam

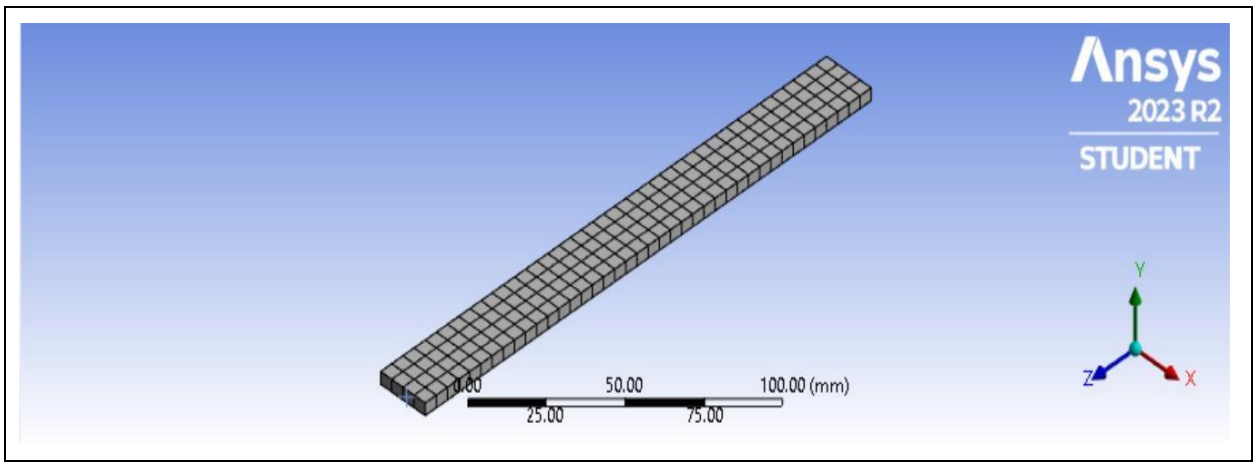

Fig. 2: Meshed uniform beam

Table 1. Aluminium alloy, wrought, 6061, T6

Density	2.713e-006 kg mm^-3
Tensile Yield Strength	259.2 MPa
Tensile Ultimate Strength	313.1 MPa
Coefficient of Thermal Expansion	2.278e-005 C^-1
Thermal Conductivity	0.1553 W mm^-1 C^-1
Specific Heat	9.157e+005 mJ kg^-1 C^-1
Resistivity	3.999e-005 ohm mm
Young's Modulus MPa	69040
Poisson's Ratio	0.33
Bulk Modulus MPa	67686
Shear Modulus MPa	25955
Temperature C	23

Based on the data presented in Table 2, it was clear that there exist some differences between the frequency obtained from ANSYS simulation and analytical calculation.

2.2 State Space Model of the Cantilever Beam

Since the dynamic of FE model has large number of degrees of freedom, a truncated modal matrix $[\varphi]$ was introduced to reduce the model order and as a result the computation cost was reduced. So, the nodal displacement vector {q} could be transformed to the reduced vector $\{\kappa\}$ as given below:

$$\{q\} = [\varphi] \tag{8}$$

Table 2. Comparison between frequencies obtained from ANSYS and analytical calculation

S. No.	Frequency from Ansys	Frequency from analytical calculation	Error (%)
1	82.237	82.152	0.0010
2	405.41	405.32	0.0002
3	514.44	514.36	0.00001
4	1437.5	1437.30	0.00013
5	1461.1	1460.12	0.0006

Therefore, the new states could be measured from the previous displacement vectors {q} and the truncated matrix which was defined as the first n modes shape matrix. By considering the first two bending mode vibration of the beam, the truncated matrix was formed by the eigenvectors of the first two modes. Thus, {q} will be (20×1) displacement vector, $[\varphi]$ will be (20×2) truncated matrix and $\{\kappa\}$ will be (2×1) modal coordinate vector.

We could obtain the decomposed equation of motion by substituting (21) into (16) and multiplying the equation by the transposed modal matrix as:

$$[\mathrm{M}']\{\ddot{\kappa}\} + [\mathrm{C}']\{\dot{\kappa}\} + [\mathrm{K}']\{\kappa\} = \{\mathrm{F}'_{\mathrm{Dist}}\}\{\mathrm{F}'_{\mathrm{Actu}}\} \tag{9}$$

where $[\mathrm{M}'], [\mathrm{C}']$ and $[\mathrm{K}']$ denote the modal mass, damping and stiffness matrices, $\{\mathrm{F}'_{\mathrm{Dist}}\}$ is the modal external force vector and $\{\mathrm{F}'_{\mathrm{Actu}}\}$ is the modal control force vector.

Therefore, state vector could be defined as

$$\{\mathbf{x}\}\begin{Bmatrix}\kappa\\ \dot{\kappa}\end{Bmatrix} \tag{10}$$

Concerning smart structures, the system input is actuation voltages, and the system output could be sensor voltages or displacements.

$$\dot{\mathrm{x}}(\mathrm{t}) = \mathrm{Ax}(\mathrm{t}) + \mathrm{B}V_a(t) \tag{11}$$
$$y(t) = \mathrm{Cx}(\mathrm{t}) \tag{12}$$
$$V_s(t) = \mathrm{Dx}(\mathrm{t}) \tag{13}$$

Therefore, matrices of the state space equation for the smart beam could be derived as:

$$[\mathrm{A}] = \begin{bmatrix}[0] & [0]\\ -[M']^{-1}[K'] & -[M']^{-1}[C']\end{bmatrix} \tag{14}$$
$$[\mathrm{B}] = \begin{bmatrix}\{0\}\\ -[M']^{-1}[\varphi]^{\mathrm{T}}\{P\}\end{bmatrix} \tag{15}$$
$$[\mathrm{C}] = [[\varphi] \quad \{0\}] \tag{16}$$
$$[\mathrm{D}] = [\{g\}^{\mathrm{T}}[\varphi] \quad \{0\}] \tag{17}$$

where [A] denotes the system matrix, [B] is the control matrix, [C] is the displacement output matrix, [D] is the sensor output matrix.

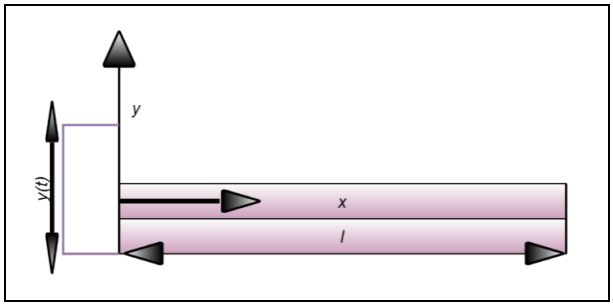

Fig. 3: Cantilever beam under base excitation

Figure 3 shows a cantilever beam system under base excitation, which is very similar to that of a constant section Euler-Bernoulli beam. The system is defined by several parameters, namely the elastic modulus (E), moment of inertia (I), and mass per unit length (m), cross-sectional area (A), and length of the beam (L). The displacement of one point on the cantilever beam under base excitation could be calculated by the following equation:

$$\lambda(x,t) = y(t) + \varphi(x,t) \tag{18}$$

where $\varphi(x,t)$ is the deflection curve, $y(t)$ is the displacement of base. If the base is in sinusoidal movement, it could be defined as $y(t) = Y\sin(\omega t)$, where ω is the radian frequency and Y is the displacement amplitude of the base movement.

If the cross-sectional strain has a linear distribution, the additional bending moment caused by the internal damping force can be written as follows:

$$M_r = \int_z \sigma_r z \, \mathrm{d}A = \int_z C_r \frac{\partial \varepsilon}{\partial t} z \, \mathrm{d}A \tag{19}$$

where z is the distance between the point of interest and the neutral surface.

From the material mechanics, the equation between strain and beam deflection can be obtained:

$$\varepsilon = -z \frac{\partial^2 \varphi(x,t)}{\partial x^2} \tag{20}$$

Substituting equation (3) into equation (2), the additional bending moment becomes:

$$Mr = \int_z c_r \frac{\partial}{\partial t}\left[-z \frac{\partial^2 \varphi(x,t)}{\partial x^2}\right] z \, \mathrm{d}A = -c_r \frac{\partial^2 \varphi(x,t)}{\partial x^2 \, \partial t} \int_z z^2 \, \mathrm{d}A = -c_r I \frac{\partial^2 \varphi(x,t)}{\partial x^2 \, \partial t} \tag{21}$$

Then the total bending moment of the small segment is:

$$M = -EI \frac{\partial^2 \varphi(x,t)}{\partial x^2} - c_r I \frac{\partial^2 \varphi(x,t)}{\partial x^2 \, \partial t} \tag{22}$$

The moment balance of the whole small segment, could yield:

$$M + \frac{\partial M}{\partial x} \, \mathrm{d}x - M - V \, \mathrm{d}x + \frac{1}{2}\left[-c \frac{\partial \lambda(x,t)}{\partial t} - m \frac{\partial^2 \lambda(x,t)}{\partial t^2}\right] (\mathrm{d}x)^2 = 0 \tag{23}$$

Neglecting the higher order term and referring to equation (5), equation (6) can be simplified as:

$$V = \frac{\partial M}{\partial x} = \frac{\partial}{\partial x}\left[-EI \frac{\partial^2 \varphi(x,t)}{\partial x^2} - c_r I \frac{\partial^2 \varphi(x,t)}{\partial x^2 \, \partial t}\right] \tag{24}$$

Further, from the force balance of the whole small segment, can yield:

$$V + \frac{\partial V}{\partial x} \, \mathrm{d}x - V - \left[m \frac{\partial^2 \lambda(x,t)}{\partial t^2} + c \frac{\partial \lambda(x,t)}{\partial t}\right] \mathrm{d}x = 0 \tag{25}$$

Substituting the expression of $\lambda(x,t)$ shown in equation (1), equation (8) becomes:

$$\frac{\partial V}{\partial x} \, \mathrm{d}x - \left[m \frac{\partial^2 y(t)}{\partial t^2} + m \frac{\partial^2 \varphi(x,t)}{\partial t^2} + c \frac{\partial y(t)}{\partial t} + c \frac{\partial \varphi(x,t)}{\partial t}\right] \mathrm{d}x = 0 \tag{26}$$

Further simplification and organization can yield:

$$\frac{\partial V}{\partial x} - m \frac{\partial^2 \varphi(x,t)}{\partial t^2} - c \frac{\partial \varphi(x,t)}{\partial t} = m \frac{\partial^2 y(t)}{\partial t^2} + c \frac{\partial y(t)}{\partial t} \tag{27}$$

At last, substituting the expression of V shown in equation (7) into equation (10) can yield the movement equation of the small segment under the base excitation, shown as:

$$EI \frac{\partial^4 \varphi(x,t)}{\partial x^4} + c_r I \frac{\partial^5 \varphi(x,t)}{\partial x^4 \, \partial t} + m \frac{\partial^2 \varphi(x,t)}{\partial t^2} + c \frac{\partial \varphi(x,t)}{\partial t} = -\left[m \frac{\partial^2 y(t)}{\partial t^2} + c \frac{\partial y(t)}{\partial t}\right] \tag{28}$$

2.3 Response Distributions of Cantilever Beam under Base Excitation

As can be seen from equation (1), any position on the cantilever beam's vibration response may be calculated if the deflection curve $\varphi(x,t)$ is known. Here, the deflection curve equation was solved using the modal superposition method $\varphi(x,t)$.

It should be noted from equation (1), if the deflection curve $\varphi(x,t)$ is known, the vibration response of any point on the cantilever beam can be determined. Here, the modal superposition method is adopted to solve the expression of the deflection curve $\varphi(x,t)$. Every order natural frequency of the beam is set as ω_i, $i = 1,2,3,\cdots$, and the relative regular modal shape function is $Y_i(x)$; it meets the following orthogonally conditions

$$\int_0^l mY_i^2(x)\mathrm{d}x = 1 \tag{29}$$

Then the deflection curve $\varphi(x,t)$ can be expressed by the regular response $\eta_i(t)$ and the regular modal shape $Y_i(x)$, shown as:

$$\varphi(x,t) = \sum_{i=1}^{\infty} Y_i(x)\eta_i(t) \tag{30}$$

For a cantilever beam, the expression of $Y_i(x)$ is:

$$Y_i(x) = D_i\left[\cosh k_i x - \cos k_i x - \frac{\sinh k_i l - \sin k_i l}{\cosh k_i l + \cos k_i l}(\sinh k_i x - \sin k_i x)\right] \tag{31}$$

where D_i is a parameter related to the excitation level, k_i is a parameter related to natural frequency. Corresponding to the first five orders, the values of k_i are 1.875/L, 4.694/L, 7.855/L, 10.996/L and 14.137/L, respectively.

Equation (11) can be solved by substituting equation (13) to obtain:

$$\sum_{i=1}^{\infty} EI\frac{\mathrm{d}^4}{\mathrm{d}x^4}Y_i(x)\eta_i(t) + \sum_{i=1}^{\infty} c_r I\frac{\mathrm{d}^4}{\mathrm{d}x^4}Y_i(x)\dot{\eta}_i(t) + \sum_{i=1}^{\infty} mY_i(x)\ddot{\eta}_i(t) = -\left[m\frac{\partial^2 y(t)}{\partial t^2} + c\frac{\partial y(t)}{\partial t}\right] \quad (31)$$

Utilizing the orthogonally conditions, equation (15) was integrated along the longitudinal direction of the beam and could become:

$$\eta_i(t)\int_0^l EI\frac{\mathrm{d}^4Y_i(x)}{\mathrm{d}x^4}Y_i(x)\mathrm{d}x + \sum_{i=1}^{\infty}\dot{\eta}_i(t)\int_0^l\left[c_r I\frac{\mathrm{d}^4Y_i(x)}{\mathrm{d}x^4} + cY_i(x)\right]Y_i(x)\mathrm{d}x + \ddot{\eta}_i(t)\int_0^l mY_i^2(x)\mathrm{d}x = F_i(t) \quad (32),$$

where $F_i(t) = \int_0^l -\left[m\frac{\partial^2 y(t)}{\partial t^2} + c\frac{\partial y(t)}{\partial t}\right]Y_i(x)\mathrm{d}x$

Assuming that the two damping coefficients c and c_r mentioned above are proportional to m and E, and expressed as $c = \alpha m, c_r = \beta E$, equation (16) can be simplified as:

$$\ddot{\eta}_i(t) + (\alpha + \beta\omega_i^2)\dot{\eta}_i(t) + \omega_i^2\eta_i(t) = F_i(t) \quad (33)$$

Accordingly, $F_i(t) = \int_0^l -\left[m\frac{\partial^2 y(t)}{\partial t^2} + \alpha m\frac{\partial y(t)}{\partial t}\right]Y_i(x)\mathrm{d}x$.

Furthermore, the i-order modal damping ratio ζ_i can be expressed as:

$$\zeta_i = \frac{\alpha + \beta\omega_i^2}{2\omega_i} = \frac{\alpha}{2\omega_i} + \frac{\beta\omega_i}{2} \quad (34)$$

Thus, the coefficients α and β can be determined from the modal damping ratio and nature frequency, the solution formulas are:

$$\alpha = \frac{2\omega_1\omega_2(\zeta_1\omega_2 - \zeta_2\omega_1)}{\omega_2^2 - \omega_1^2} \quad (35)$$

$$\beta = \frac{2(\zeta_2\omega_2 - \zeta_1\omega_1)}{\omega_2^2 - \omega_1^2} \quad (36)$$

where $\zeta_1, \zeta_2, \omega_1, \omega_2$ can be obtained from the experiment.

Combining equation (17) and equation (18) yields the final equation:

$$\ddot{\eta}_i(t) + 2\zeta_i\omega_i\dot{\eta}_i(t) + \omega_i^2\eta_i(t) = F_i(t) \quad (37)$$

The solution of equation (21) can be easily obtained by referring to a single-degree-of-freedom system shown as:

$$\eta_i(t) = \mathrm{e}^{-\zeta_i\omega_i t}\left[\frac{\dot{\eta}_{i0} + \zeta_i\omega_i\eta_{i0}}{\omega_i'}\sin\omega_i' t + \eta_{i0}\cos\omega_i' t + \frac{1}{\omega_i'}\int_0^t F_i(\tau)e^{\zeta_i\omega_i\tau}\sin\omega_i'(t - \tau)\,\mathrm{d}\tau\right] \quad (38)$$

where

$$\omega_i' = \omega_i\sqrt{1 - \zeta_i^2}$$

$$\eta_{i0} = \int_0^l m\varphi(x,0)Y_i\,\mathrm{d}x$$

$$\dot{\eta}_{i0} = \int_0^l m\dot{\varphi}(x,0)Y_i\,\mathrm{d}x$$

Finally, the total displacement of the cantilever beam under sinusoidal base excitation is expressed as:

$$\lambda(x,t) = y(t) + \varphi(x,t) = y(t) + \sum_{i=1}^{\infty} Y_i(x)\eta_i(t) \quad (39)$$

From equation (39), the response distributions of cantilever beam under base excitation can be determined.

The aluminium beam 6061 T6 in a cantilever state was selected as the study object in this work. The vibration test device was an acceleration sensor of light mass, and the base excitation device was a shaking table. The experiment system was then built (depicted in Fig. 4), and the mode shapes of the first five natural frequencies are shown in Fig. 5.

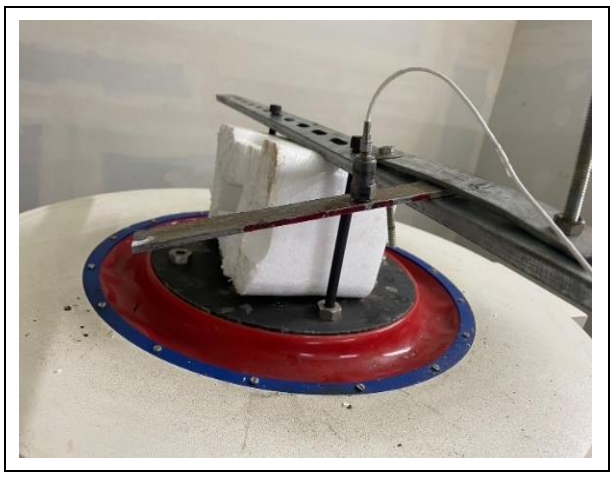

Fig. 4: Experimental setup of aluminium 6061 T6 beam

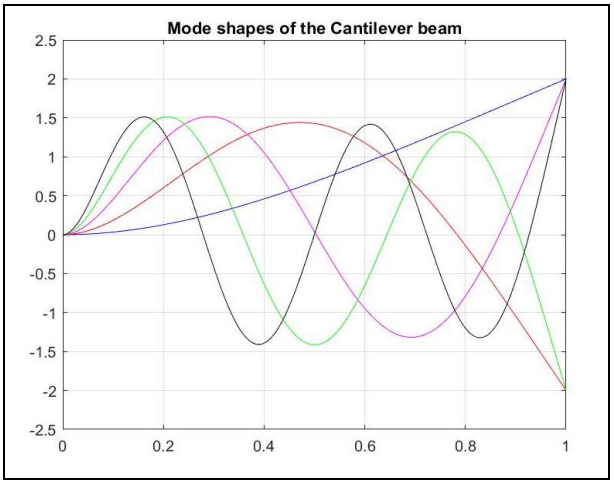

Fig. 5: Mode shapes of the cantilever beam

A block diagram showcasing the vibration shaker experimental setup is presented in Fig. 6. The components are as follows:

- **Vibration Shaker**: This is the primary component of the experimental setup. It is responsible for generating the vibration or shaking motion required for the experiment.
- **Amplifier**: The amplifier is used to increase the voltage signal from the signal generator to a level suitable for driving the vibration shaker. It is important to choose an amplifier compatible with the signal generator and vibration shaker.
- **Signal Generator**: The signal generator produces an electrical signal that is used to control the vibration shaker. It is crucial to select a signal generator that is capable of providing the required frequency range and amplitude for the experiment.
- **Power Amplifier**: The purpose of the power amplifier is to provide the necessary power to the vibration shaker without distortion.
- **Data Acquisition System (DAQ)**: The DAQ system is used to measure and record the data obtained from the experiment. This system is chosen based on the type of data to be collected and the frequency range of the experiment.
- **Sensors**: Sensors are used to measure various parameters during the experiment such as acceleration, displacement, and velocity. It is essential to select sensors compatible with the vibration shaker and data acquisition system.

Figure 7 shows the block diagram setup of the system.

3. RESULTS AND DISCUSSIONS

3.1 Response Test of the Cantilever Beam

The cantilever beam has two measuring points fitted in accordance with the analysis. Through shaker excitation, natural frequencies and modal damping ratios were obtained. Table 3 lists the modal damping ratios. Additionally, base excitation was performed at the frequencies and levels specified in the analysis to produce responses for the two designated points.

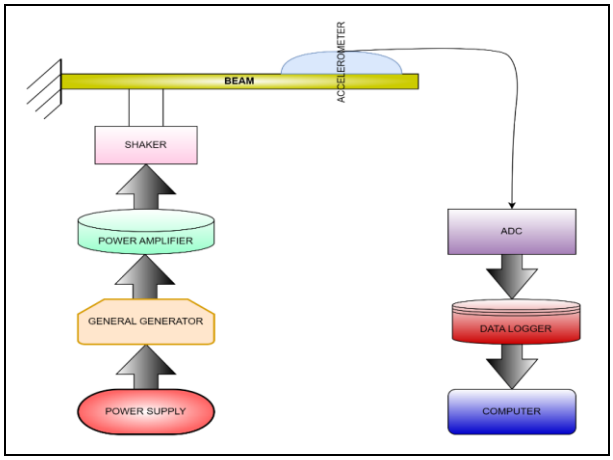

Fig. 6: Block diagram of the experimental system

Table 3. Modal damping ratios of the beam

1	2	3	4	5
0.393	0.035	0.019	0.013	0.022

When analysing the response of a cantilever beam under base excitation, it is important to consider the accuracy of the experiment and analysis. Upon review, it was discovered that there was little difference between the two methods. In fact, the maximum difference was

smaller for the same exciting frequencies, indicating consistency between the two. This validates the proposed response analysis method. However, at a specific location, the difference between analysis and experiment was greater than other points. This may be due to an inaccurate vibration pickup point. To confirm, the pickup point was modified and the analysis was repeated. The results are listed in Table 4 for comparison.

Table 4 shows that adjusting the value in the vicinity of x=0.1 results in a smaller difference between the calculated values and the experimental data. This suggests that the inaccurate distance was the primary source of variation between the experimental and theoretical analysis at the location of x=0.

3.2 Positive Position Feedback (PPF) Controller Design

In terms of stability, durability, and simplicity of installation, PPF controller design is one of the more beneficial controller design techniques. Studies on the dampening or suppression of vibration can efficiently employ this controller architecture. In addition to serving as an auxiliary system like a mechanical vibration damper, the PPF controller also serves as a compensation. A single target mode was damped in the narrow frequency band if the controller architecture contained only one compensator. In the broad frequency range, multimodal control was attained if the right number of parallel compensators were used. Through the use of the system's relevant dynamic properties, the compensators, or second-order transfer functions, for the PPF are designed in the controller. The compensator of the single PPF method is given in equation (1), where ξ_n, ω_n, and K are the damping ratio, the natural frequency, and the gain parameters, respectively. The PPF controller for the multimodal control's second-order transfer functions are generated using the first three modes of the smart beam. The damping ratio and the gain factor for first three modes of the smart beam are chosen as $\xi_n = 0.02$ and $K = 10^7$, respectively.

Table 4. Response of the beam when excitation frequency was 200 Hz

Exciting level	0.3 g	0.8 g
Calculated value A(x = 0.096 m)	1.00	2.60
Measured value B	1.01	2.68
Difference $\lvert A-B\rvert/B$(%)	0.99	2.99

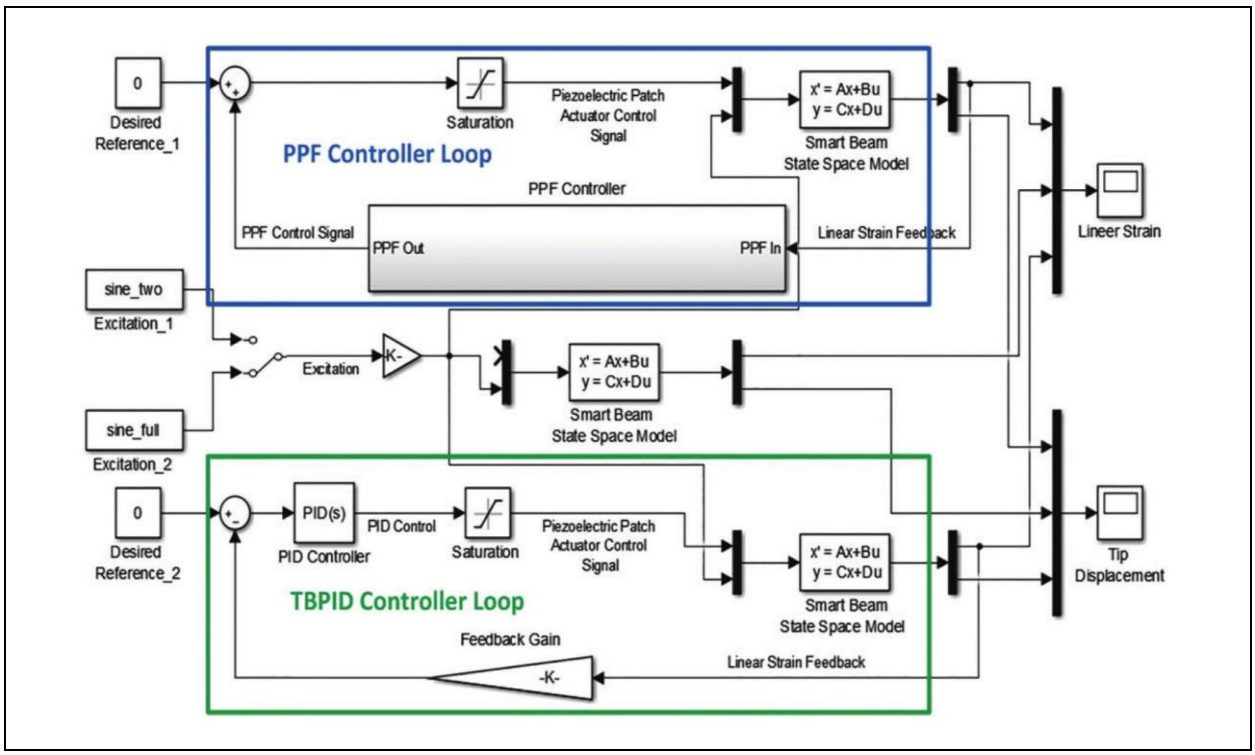

Fig. 7: Block diagram of the system

Table 5. The evaluation of the presented controller designs

Controller	Under the sine-two excitation RMS values		Under the sine-three excitation RMS values	
	Strain (mm/mm)	Tip displacement (mm)	Strain (mm/mm)	Tip displacement (mm)
Uncontrolled	1.47×10^{-3}	32.28	1.47×10^{-3}	16.19
PPF	0.6×10^{-3}	13.76	0.7×10^{-3}	5.8
TBPID	0.35×10^{-3}	3.79	0.49×10^{-3}	---------
PPF	481.1	540.3	--------	----------
TBPID	363.2	503.7	--------	----------

TBPID: Tuner-Based Proportional-Integral-Derivative; PPF: Positive Position Feedback.

$$H(s)_n = \frac{K}{s^2 + 2\xi_n \omega_n s + \omega_n^2}$$

The transfer functions for the three modes are derived from equation (1). Then, they are applied parallel to the control loop as positive feedback with the help of the determined coefficients that can be tuned.

3.3 TBPID Controller Design

The PID controller design is the simplest controller in terms of easy installation and robust performance. In order to optimize the controller's closed-loop performance, three PID parameters need to be adjusted based on the boundary conditions. To obtain suitable PID parameters, a tuner-based PID (TBPID) controller design was employed using MATLAB/Simulink/Control System Tuner toolbox. First, in the toolbox, two blocks (PID, feedback gain) are selected in order to tune the parameters. The transient goal method that includes the impulse signal was also used to achieve better controller performance. The reference model was selected as a second-order transfer function. The tuning parameters of the PID controller were optimized as $K_p = -3664.08, K_i = 4.7\text{e}-06$, and $K_d = 8.03$. The filter coefficient (N) was obtained as $N = 988.55$. A feedback gain $(FG = 275.27)$ was used from the output of the system. These parameters providing the best controller performance were demonstrated by the results of a series of closed-loop tests.

3.4 Evaluating Controller Performance for Proposed Designs

Figure 7 illustrates the block diagram of the proposed controller designs for active vibration control in MATLAB/Simulink. To achieve collocated control, strain responses were utilized as feedback instead of tip displacement, which were affected by signal source location. The TBPID and PPF controllers were designed to achieve this goal. The performance of the controller designs was assessed using both tip displacement and strain response. The system was excited by both sine-two and sine-three waves, and the controller designs were evaluated through simulations. The RMS values of the results were analysed to determine the reduction in control level, as it was the most effective measure of amplitude, taking into account the time history of the wave.

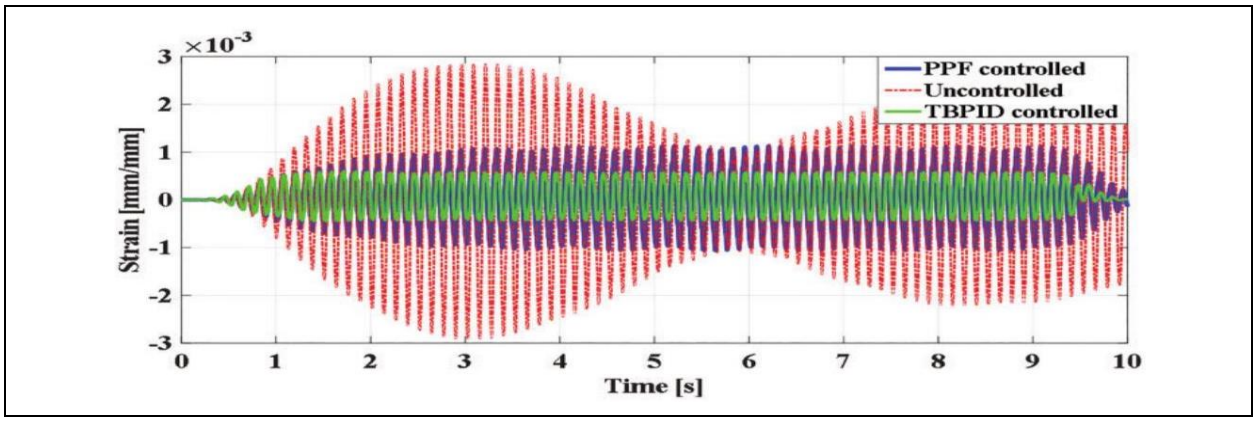

Fig. 8: Strain response under the sine-two excitation. PPF: positive position feedback; TBPID: tuner-based PID

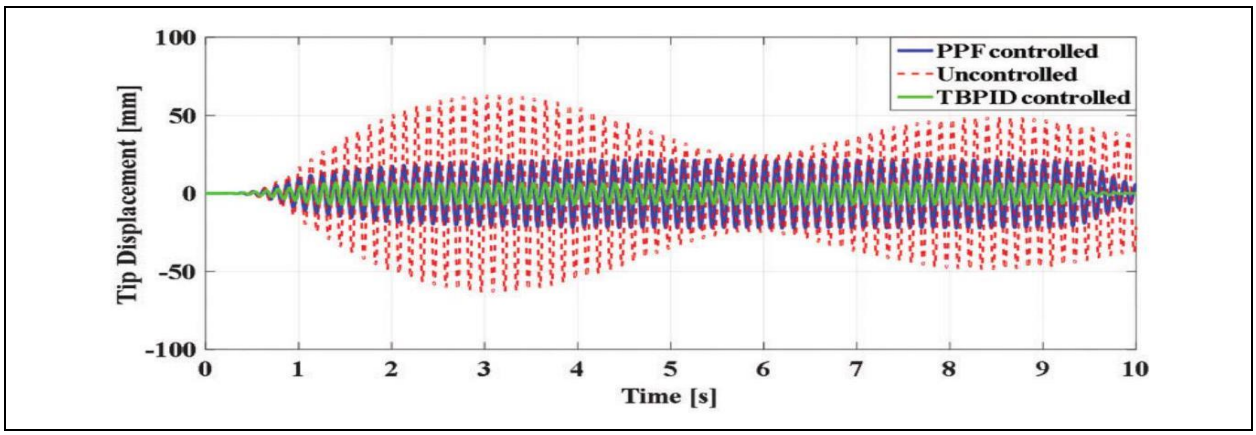

Fig. 9: Tip displacement response under the sine-two excitation. PPF: positive position feedback; TBPID: tuner-based PID

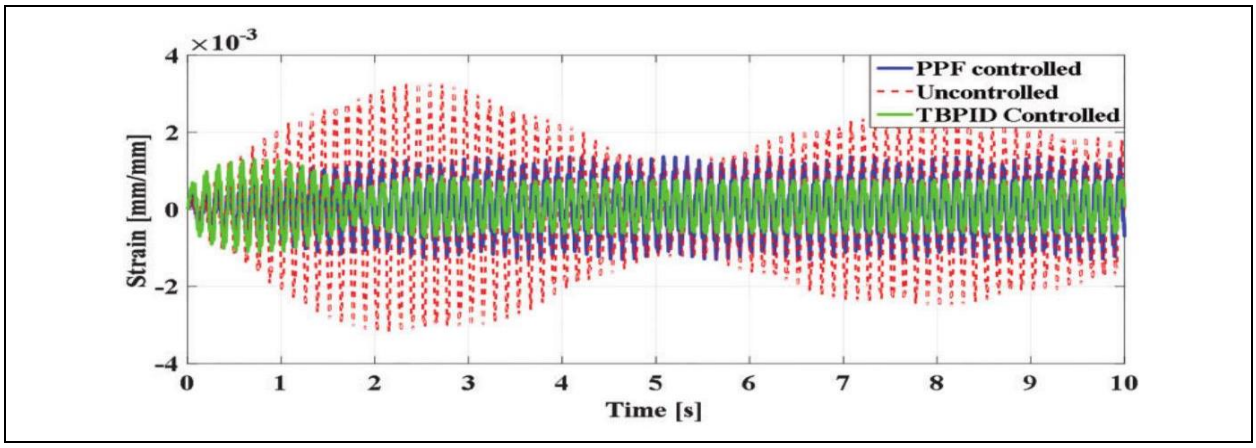

Fig. 10: Strain response under the sine-three excitation. PPF: positive position feedback; TBPID tuner-based PID

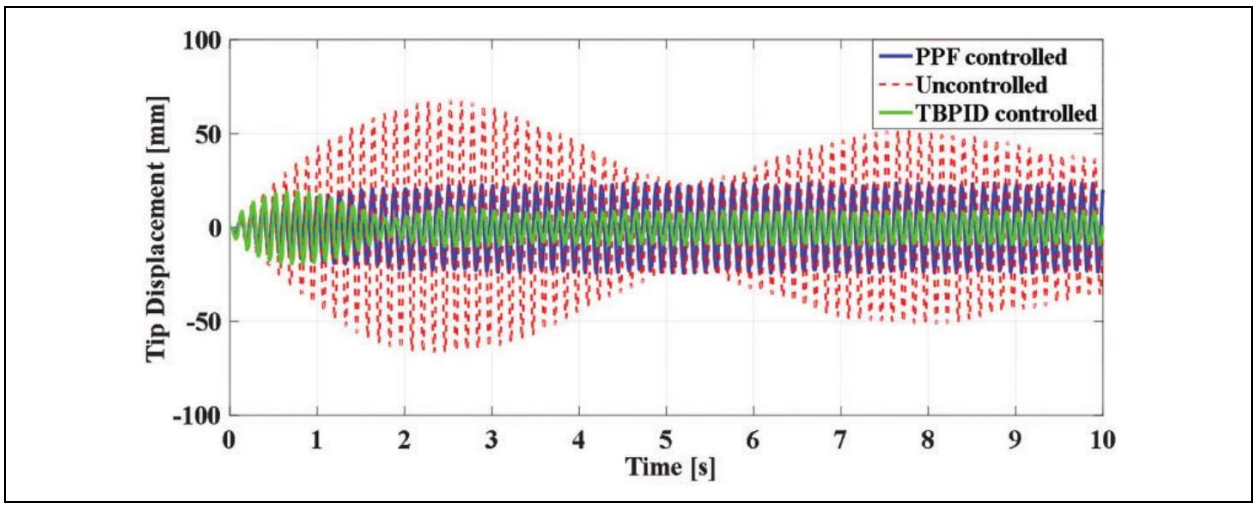

Fig. 11: Tip displacement response under the sine-three excitation. PPF: positive position feedback; TBPID: tuner-based PID

The impact of the controller designs presented here on the system is illustrated in Figures 8 to 11, and the corresponding RMS values are shown in Table 5. The results demonstrate that active forced vibration control of the system, using PPF and TBPID techniques, was successful. Under sine-two excitation, the forced

vibrations of controlled systems were suppressed by approximately 60, in comparison to the uncontrolled strain response, for both PPF and TBPID controllers.

4. CONCLUSION

This study examines the effectiveness of TBPID and PPF controllers in reducing force vibrations in smart beams that utilize piezoelectric actuators. The numerical results indicate that for forced vibration control, the overall TBPID control performance was more effective than that of the PPF-controlled system. However, for free vibration control, the PPF controller outperforms the PID-based controllers. Additionally, the RMS values of the control signal were analysed to evaluate controller power consumption. The TBPID controller was found to provide increased energy savings compared to the PPF controller for all controllers presented in this study. In future work, the TBPID controller design could be used to control vibrations in helicopter fuselage systems during flight tests, with the aim of reducing the interior noise level of the aircraft. Another aspect of this paper involves the analysis of the response calculation of cantilever beams under base excitation. The vibration response distributions of the cantilever beam at base excitation were solved using the modal superposition method, while the movement equation of the cantilever beam was obtained utilizing moment and force equilibrium. Investigating the mechanical properties and vibration behaviours of Cantilever Beam 6061T6, the state space approach method and frequency distribution under base excitation approach were implemented. By comparing the results, we confirm that both the methods produced similar outcomes, indicating that the state space approach is a useful tool for exploring the characteristics of nanomaterials. Additionally, the continuum mechanics approach could accurately predict the mechanical properties of the beam. Our findings also demonstrated that the frequencies rely on the SW defect density and have a one-to-one relationship with additional mass and applied strain. Consequently, vibration control in nanomaterials could be regulated to develop practical applications in nano-mass and nano-strain sensors by measuring frequencies. Overall, nanotechnology has a vast potential for wider application in vibration control. The proposed method provides insight into the dynamics mechanism of structures under base excitation and could be used as a reference for the dynamic analysis of similar structures.

FUNDING

This research received no specific grant from any funding agency in the public, commercial, or not-for-profit sectors.

CONFLICTS OF INTEREST

The authors declare that there is no conflict of interest.

COPYRIGHT

REFERENCES

Avcar, M., Free vibration analysis of beams considering different geometric characteristics and boundary conditions, *J. mech. appl.*, 4(3), 94–100 (2014). http://dx.doi.org/10.5923/j.mechanics.20140403.03

Choi, S. B. and Sohn, J. W., Chattering alleviation in vibration control of smart beam structures using piezofilm actuators, experimental verification, *J. Sound Vib.*, 294(3), 640–649 (2006). https://doi.org/10.1016/j.jsv.2005.12.026

Flatau, A. B. and Chong, K. P., Dynamic smart material and structural systems, *Eng. Struct.*, 24(3), 261-270 (2002). http://dx.doi.org/10.1016/S0141-0296(01)00093-1

Gatti, G., Brennan, M. J. and Gardonio, P., Active damping of a beam using a physically collocated accelerometer and piezoelectric patch actuator, *J. Sound Vib.*, 303(3-5), 798-813 (2007). http://dx.doi.org/10.1016/j.jsv.2007.02.006

Heganna, S. and Joglekar, J., Active vibration control of smart structure using PZT patches, twelfth international multiconference on information processing, *Procedia Comput. Sci.*, 89, 710–715 (2016). http://dx.doi.org/10.1016/j.procs.2016.06.040

Kamile, S., Introduction, classification and applications of smart materials: an overview, *Am. J. Appl. Sci.*, 10(8), 876-880 (2013). https://doi.org/10.3844/ajassp.2013.876.880

Kapuria, S. and Kulkarni, S., An efficient quadrilateral element based on improved zigzag theory for dynamic analysis of hybrid plates with electrode piezoelectric actuators and sensors, *J. Sound Vib.*, 315 (1–2), 118–145, (2008). http://doi.org/10.1016/j.jsv.2008.01.053

Khalil, I. and Abdel, B. S., A hybrid PID control scheme for flexible joint manipulators and a comparison with sliding mode control, *Ain Shams Eng. J.*, 9, 3451–3457 (2018). https://doi.org/10.1016/j.asej.2018.01.004

Khot, S. M., Yelve, N. P., Tomar, R., Desai, S. and Vittal, S., Active vibration control of cantilever beam by using PID based output feedback controller, *J. Vib. Control*, 18(3), 366–372 (2012). http://dx.doi.org/10.1177/1077546311406307

Kozupa, M. and Wiciak, J., Active Vibration Control of Rectangular Plate with Distributed Piezo-elements Excited Acoustically and Mechanically, *Acta Phys. Pol. A*, 118, 95–98 (2010). http://doi.org/10.12693/APhysPolA.118.95

Krishna, J. G. and Thirumal, J. R., Application of smart materials in smart structures, *Int. J. Innovat. Res. Sci. Eng. Technol.*, 4(7), 5018–5023, (2015). https://doi.org/10.15680/IJIRSET.2015.0407206

Qiu, C. Z., Han, D. J., Zhang, M. X., Wang, C. Y. and Wu, W. Z., Active vibration control of a flexible beam using a non-collocated acceleration sensor and piezoelectric patch actuator, *J. Sound Vib*., 326(3-5), 438-455 (2009). https://doi.org/10.1016/j.jsv.2009.05.034

Rahman, N. and Alam, M. N., Structural control of piezoelectric laminated beams under thermal load, *J. Therm. Stresses*, 38(1), 69–95 (2015). http://dx.doi.org/10.1080/01495739.2014.976138

Rahman, T. A. Z. and Darus, I. Z. M., Experimental Evaluation of Active Vibration Control of a Flexible Plate using Proportional Gain Controller, *IEEE Symposium on Industrial Electronics and Applications*, 382-386 (2011). http://doi.org/10.1109/ISIEA.2011.6108736

Sarhan, M. M., Computational Finite Element Methods in Nanotechnology, 1st Ed., CRC Press (2013). https://doi.org/10.1201/b13002

Sukesha, R. V. and Kumar, N., Active vibration control of a cantilevered plate instrumented with piezoelectric patches: robust to variations in electric field, *2014 Recent Advances in Engineering and Computational Sciences*, 1-5 (2014). http://dx.doi.org/10.1109/RAECS.2014.6799522

Wei, S. and Ying, L., Determination of the response distributions of cantilever beam under sinusoidal base excitation, *J. Phys. Conf. Ser*., 448(1), 1-11 (2010). http://dx.doi.org/10.1088/1742-6596/448/1/012010

Yin, Y. and Xiong, J., Finite element analysis of electrospun nanofibrous mats under biaxial tension, *Nanomater*., 8(5), 1-19 (2018). https://doi.org/10.3390/nano8050348